BMC Ophthalmology

RESEARCH Open Access

Elevated hyperreflective foci as a novel characteristic in idiopathic epiretinal membrane by optical coherence tomography angiography

Shuyu Zhao[1,2], Xianjun Liang[2], Jinxian He[2], Yanchun Wu[2] and Jinglin Zhang[1*]

Abstract

Purpose The objective of this study was to analyze hyperreflective foci at the vitreous-retinal interface in cases of idiopathic epiretinal membrane (iERM) using enface-OCT.

Methods This study included 47 patients (52 eyes) diagnosed with iERM between January 2020 and July 2023. We observed changes in hyperreflective foci in the macular area at each stage of iERM using OCTA on a 6 mm slab of the VRI. Evaluations included the density and percentage of hyperreflective foci of the epiretinal membrane at each stage, as well as the relationship between hyperreflective foci density and other OCT parameters, such as macular thickness and changes in macular superficial vascular density.

Results Statistically significant differences in hyperreflective foci density and percentage were observed across the four stages of patients ($p < 0.05$). Additionally, statistically significant differences in superficial vascular density were noted among the four stages ($p < 0.05$). Hyperreflective foci area percentage and density correlated significantly with hyperreflective foci, FAZ area, and FAZ perimeter ($p < 0.005$). However, no correlation was found between hyperreflective foci density and area percentage with superficial vascular density and superficial perfusion density ($p > 0.05$).

Conclusion Hyperreflective foci were identified in all stages of iERM, with their number and density increasing as the disease progressed.

Keywords Idiopathic epiretinal membrane, Optical coherence tomography, OCT-angiography, Hyperreflective foci

*Correspondence:
Jinglin Zhang
zhjinglin@126.com
[1]Aier Eye Hospital, Jinan University, No. 191, Huanshi Middle Road, Yuexiu District, Guangzhou, Guangdong, PR China
[2]Foshan Aier Eye Hospital, Foshan, Guangdong, PR China

Introduction

Idiopathic Epiretinal Membrane (iERM) is a fibrous cellular membrane arising from a multifactorial etiological factors, which leads to cell proliferation on the retinal surface in the macular area. In its early stages, symptoms of visual deterioration may not be apparent [1]. However, when the condition affects the central fovea of the macula, it can cause visual impairment, distorted visual, and functional changes. It is also associated with disturbances in retinal hemodynamics. Epidemiological studies sugges that the iERM affects approximately 9.1% of the global population [2]. While the precise mechanisms underpinning iERM are not fully understood, it is likely linked to posterior vitreous detachment (PVD), which damage the internal limiting membrane (ILM) [3], and triggers the activation and migration of retinal pigment epithelium (RPE) cells, glial cells, and transparent cells towards the ILM. Additionally, the residual vitreous cortex on the retinal surface may act as a scaffold for inflammatory related cellular migration and proliferation, thereby fostering the formation of ERM.

Although iERM differs from inflammatory retinal diseases such as retinal vasculitis, evidence suggests an inflammatory response is involved in its pathogenesis. Hyperreflective foci, represent a distinctive inflammatory phenotype, comprising microglial cells, perivascular macrophages, macrophages derived from monocytes, and a subset of vitreous-resident cells [4]. Microglial cells, predominantly situated within the retinal tissues in the inner and outer plexiform layers, coexist with perivascular macrophages, which surround retinal blood vessels in the retinal nerve fiber layer and possess the potential to exhibit characteristics [5]. Both microglial cells and perivascular macrophages assume pivotal roles in preserving retinal vascular homeostasis and the integrity of the blood-retinal barrier. However, in cases of inflammation and blood-retinal barrier breakdown, monocyte-derived macrophages can be induced to infiltrate the retina [6]. Considering that hyperreflective foci are a distinctive population of cells found at the vitreoretinal interface by optical coherence tomography angiography (OCTA), this study used OCTA to perform enface imaging in patients with iERM to determine the imaging features associated with hyperreflective foci.

Materials and methods

Subjects

This retrospective study comprised a cohort of 47 patients (52 eyes) diagnosed with iERM at Aier Eye Hospital between January 2020 and July 2023. The study was approved by the Ethics Committee at AIER Eye Hospital of Foshan (2023-IRB6), and adhered to the Declaration of Helsinki's principles. Informed consent was obtained from all participants. Patients underwent fundus examination, fluorescein angiography (FFA), optical coherence tomography (OCT), and OCT angiography (OCTA). We also recorded best-corrected visual acuity (BCVA), intraocular pressure (IOP) and axial length (AL) for each eye. Exclusion criteria included: (1) Age-related macular degeneration; (2) Choroidal neovascularization from any cause; (3) Diabetic retinopathy; (4) Retinal artery or vein occlusion; (5) History of retinal detachment; (6) Tractional macular schisis; (7) Glaucoma or optic nerve disorders; (8) Ocular inflammation; (9) History of endophthalmitis or other intraocular infection; (10) History of intraocular surgery other than uncomplicated cataract phacoemulsification; (11) intravitreal injections or retinal laser photocoagulation within the past 6 months; (12) History of ocular or systemic trauma; (13) History of diabetes.

OCT imaging

All patients underwent Spectralis spectral domain-optical coherence tomography (SD-OCT; Heidelberg Engineering GmbH, Heidelberg, Germany) to assess their condition. The ectopic inner foveal layers (EIFL) was observed using SD-OCT. The epiretinal membrane was observed as continuous hyporeflective and hyperreflective bands extending from the inner nuclear layer (INL) and inner plexiform layer to the central fovea. The iERM cases were classified into four stages based on the severity of the disease [7]. Stage I was featured mild morphological or anatomical disruption. In stage II involved loss of foveal depression without EIFL. Stage III presented a continuous EIFL across the central fovea. Stage IV was indicated by a continuous EIFL with anatomical macular disruption. Central macular thickness (CMT) was measured as the mean distance between the inner limiting membrane (ILM) and the retinal pigment epithelium (RPE) within a 1 mm diameter centred on the fovea.

OCTA imaging

High-density (HD) macular angiography images were obtained using the Cirrus HD-OCT 5000 (Carl Zeiss Meditec Inc, Dublin, CA, USA) with a 6 × 6 mm scan centered on the fovea. In cases of deviation from the appropriate scanning position, manual corrections were made. Images with motion artifacts or a quality score less than 5 were excluded. The built-in software quantified the superficial vascular density and perfusion density within a 6 × 6 mm area centered on the fovea, according to the Early Treatment Diabetic Retinopathy Study (ETDRS) grid [8]. The en face OCT images were manually adjusted to set a custom slab from the epiretinal membrane to 6 μm below the ILM in the macular region for further processing.

Quantification of hyperreflective foci

The en face images from the 6 × 6 mm OCTA scans were imported into ImageJ (National Institutes of Health, Bethesda, MD, USA). The hyperreflective foci layer OCT slab underwent a Gaussian blur (sigma 5.0) followed by an inverse transformation. The resulting blurred and inverted image was combines with the original image. A rolling ball background subtraction with a radius of 5 pixels corrected for smaller areas of background irregularity. Any remaining superficial vessel artifacts were manually removed, resulting in the 'background-subtracted' image [9]. Signal enhancement facilitated cell identification. Binary thresholding was used to extract discrete cell shapes. The density of hyperreflective foci and the percentage of area occupied by these foci were quantified using the "Analyze Particles" function. Hyperreflective foci density was calculated by dividing the number of cells by the total image area (cells/mm^2) (Fig. 1**).**

Statistical analysis

The statistical software used for data analysis was SPSS 23.0 (IBM Corp., Armonk, NY, USA). All continuous data were presented as mean ± standard deviation (X ± s). A one-way analysis of variance (ANOVA) was utilized to examine the parameters, including CMT, foveal avascular zone (FAZ) area, FAZ perimeter, superficial vascular density, superficial perfusion density, hyperreflective foci density, and hyperreflective foci percentage, across various iERM grades. Subsequently, pairwise comparisons were conducted using the "emmeans" function. Considering the presence of intra-group correlation in the eyes, this study employed a generalized estimating equation to carry out statistical analysis of CMT, FAZ_area, FAZ_perimeter, SVD, SPD, hyperreflective foci indexes of the four groups. To ensure accuracy, the impact of age and pvd were adjusted for during the analysis. Categorical data were presented as counts (%) and comparisons among groups were made using a chi-square test. Pearson's correlation coefficients were used to assess the linear relationship between different factors and hyperreflective foci. ggplot2 was utilized to create appropriate graphs. A significance level of $P < 0.05$ was deemed statistically significant.

Results

Baseline characteristics

Accordaning to the predetermined inclusion and exclusion criteria, a total of 47 individuals (52 eyes) were enrolled in this study. Among them, there were 13 males (18 eyes) and 34 females (34 eyes), with an average age of 67.21 ± 9.11 years. The cohort included 11 eyes classified as Stage I, with an average age of 63.91 ± 12.24 years. Additionally, 14 eyes were classified as Stage II, with an average age of 68.64 ± 7.37 years. 15 eyes were categorized as Stage III, with an average age of 66.73 ± 8.38 years and a male-to-female ratio of 4:9. Finally, 12 eyes were designated as Stage IV, with an average age of 69.17 ± 8.80 years. The conducted statistical analysis examining the basic characteristics of the four stages did not reveal any significant differences ($P > 0.05$) regarding eye laterality, age, gender, intraocular pressure (IOP), or axial length (AL). However, there was a statistically significant

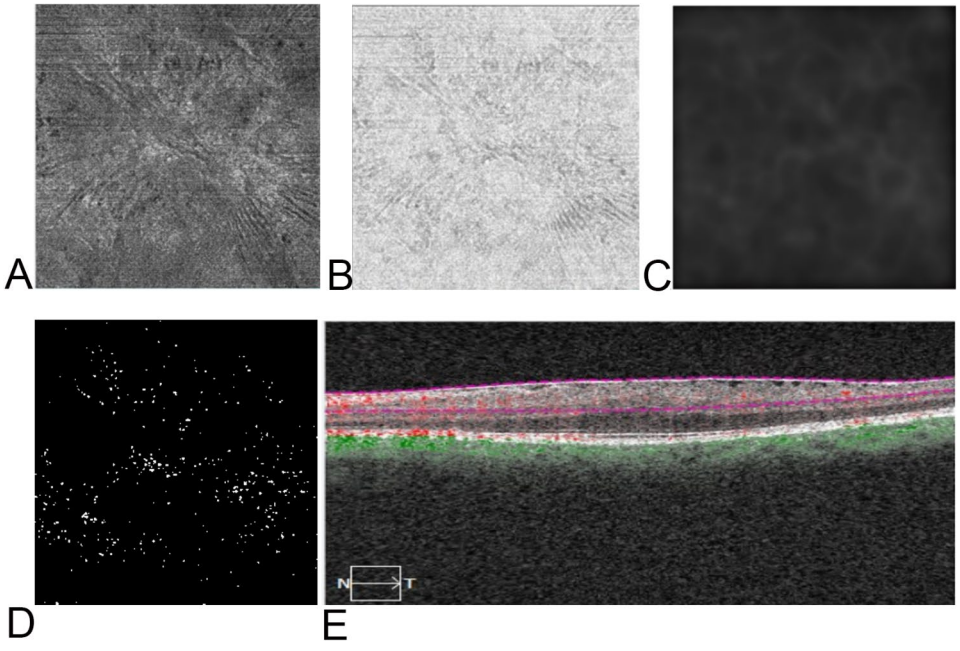

Fig. 1 **A**: 6 μm OCTA enface image above the ILM, showing high reflectivity points representing the hyperreflective foci. **B**: Import enface image into imageJ and remove the background. **C**: Gaussian blur the image. **D**: Threshold the image to extract discrete cell shapes. **E**: OCT image of the iERM

Table 1 Baseline characteristics of patients with iERM at all stages

Variables	Total (*n* = 52)	I (*n* = 11)	II (*n* = 14)	III (*n* = 15)	IV (*n* = 12)	*p*
eye, n (%)						0.701
od	26 (50)	7 (63.6)	7 (50)	6 (40)	6 (50)	
os	26 (50)	4 (36.4)	7 (50)	9 (60)	6 (50)	
age, Mean ± SD	67.21 ± 9.11	63.91 ± 12.24	68.64 ± 7.37	66.73 ± 8.38	69.17 ± 8.80	0.509
gender, n (%)						0.610
female	34 (65.4)	9 (81.8)	8 (57.1)	9 (60)	8 (66.7)	
male	18 (34.6)	2 (18.2)	6 (42.9)	6 (40)	4 (33.3)	
pvd, n (%)						< 0.001
no	20 (38.5)	9 (81.8)	9 (64.3)	2 (13.3)	0 (0)	
yes	32 (61.5)	2 (18.2)	5 (35.7)	13 (86.7)	12 (100)	
IOP, Mean ± SD	14.15 ± 1.47	14.45 ± 1.57	14.14 ± 1.56	13.87 ± 1.60	14.25 ± 1.22	0.792
AL, Mean ± SD	23.42 ± 0.96	23.70 ± 0.93	23.24 ± 1.03	23.35 ± 1.12	23.46 ± 0.70	0.694

IOP: intraocular pressure, AL: The axial length, PVD: posterior vitreous detachment

Table 2 Hyperreflective foci and OCTA parameters with iERM at all stages

Variables	I (*n* = 11)	II (*n* = 14)	III (*n* = 15)	IV (*n* = 12)	*p*
CMT (mm)	285.82 ± 36.60	352.79 ± 34.23	454.67 ± 37.59	550.00 ± 59.30	< 0.001
FAZ_area (mm^2)	0.25 ± 0.11	0.16 ± 0.09	0.07 ± 0.04	0.06 ± 0.03	< 0.001
FAZ_perimeter (mm^{-1})	2.28 ± 0.54	1.71 ± 0.28	1.13 ± 0.49	0.94 ± 0.26	< 0.001
SVD (mm^{-1})	16.03 ± 2.07	16.22 ± 2.03	16.77 ± 2.27	17.13 ± 1.17	0.493
SPD	0.39 ± 0.05	0.39 ± 0.05	0.42 ± 0.06	0.43 ± 0.03	0.131
hyperreflective foci counts (cells)	208.82 ± 43.22	281.86 ± 53.46	414.53 ± 42.96	531.83 ± 118.94	< 0.001
hyperreflective foci _percentage (%)	0.32 ± 0.15	0.45 ± 0.17	0.83 ± 0.50	1.18 ± 0.91	< 0.001
hyperreflective foci _density (cells/mm^2)	5.84 ± 1.22	7.83 ± 1.48	11.51 ± 1.19	14.77 ± 3.30	< 0.001

CMT: Central Macular Thickness, FAZ: foveal avascular zone, SVD: superficial vascular density, SPD: superficial perfusion density

difference ($P < 0.001$) among the four groups in terms of PVD. The proportion of PVD gradually increased with the higher stages (I-IV)(Table 1).

Hyperreflective foci and OCTA parameters in different stages of idiopathic epiretinal membrane patients

In terms of CMT across the four stages, Stage I exhibited a CMT of 285.82 ± 36.60, Stage II had 352.79 ± 34.23, Stage III had 454.67 ± 37.59, and Stage IV had 550.00 ± 59.30. Statistical analysis revealed significant differences in CMT among the four stages ($p < 0.05$). The comparison of FAZ area among the four stages yielded the following results: Stage I had an area of 0.25 ± 0.11, Stage II had 0.16 ± 0.09, Stage III had 0.07 ± 0.04, and Stage IV had 0.06 ± 0.03. There were statistically significant differences in FAZ area among the four stages ($p < 0.05$). Similarly, the comparison of FAZ perimeter among the four stages revealed the following values: Stage I had a perimeter of 2.28 ± 0.54, Stage II had 1.71 ± 0.28, Stage III had 1.13 ± 0.49, and Stage IV had 0.94 ± 0.26. Statistical analysis indicated significant differences in FAZ perimeter among the four stages ($p < 0.05$).

Moving on to the comparison of superficial vascular density (SVD) among the four stages, the results were as follows: Stage I had a density of 16.03 ± 2.07, Stage II had 16.22 ± 2.03, Stage III had 16.77 ± 2.27, and Stage IV had 17.13 ± 1.17. No statistically significant differences were observed in SVD among the four stages ($p > 0.05$). Likewise, the comparison of superficial perfusion density (SPD) among the four stages yielded the following values: The density of Stage I was 0.39 ± 0.05, Stage II was 16.77 ± 2.03, Stage III was 16.77 ± 2.27 and Stage IV was 17.13 ± 1.17. There were no statistically significant differences found in SPD across the four stages ($p > 0.05$).

Turning our attention to the comparison of hyperreflective foci density among the four stages, the results were as follows: Stage I had a density of 5.84 ± 1.2, Stage II had 7.83 ± 1.48, Stage III had 11.51 ± 1.19, and Stage IV had 14.77 ± 3.30. Statistical analysis revealed significant differences in hyperreflective foci density among the four stages ($p < 0.05$). Finally, the comparison of hyperreflective foci percentage among the four stages yielded the following values: Stage I had a percentage of 0.32 ± 0.15, Stage II had 0.45 ± 0.17, Stage III had 0.83 ± 0.52, and Stage IV had 1.18 ± 0.91. ($p < 0.05$) (Table 2). Figure 2 provides a visual representation of typical examples in each stage (Fig. 2).

The study's results indicated that the levels of hyperreflective foci index increased progressively with each stage. The statistical analysis confirmed significant differences for hyperreflective foci counts and hyperreflective foci density between all four stages. However, no statistically significant differences in hyperreflective foci percentage were observed between Stage III and Stage IV.

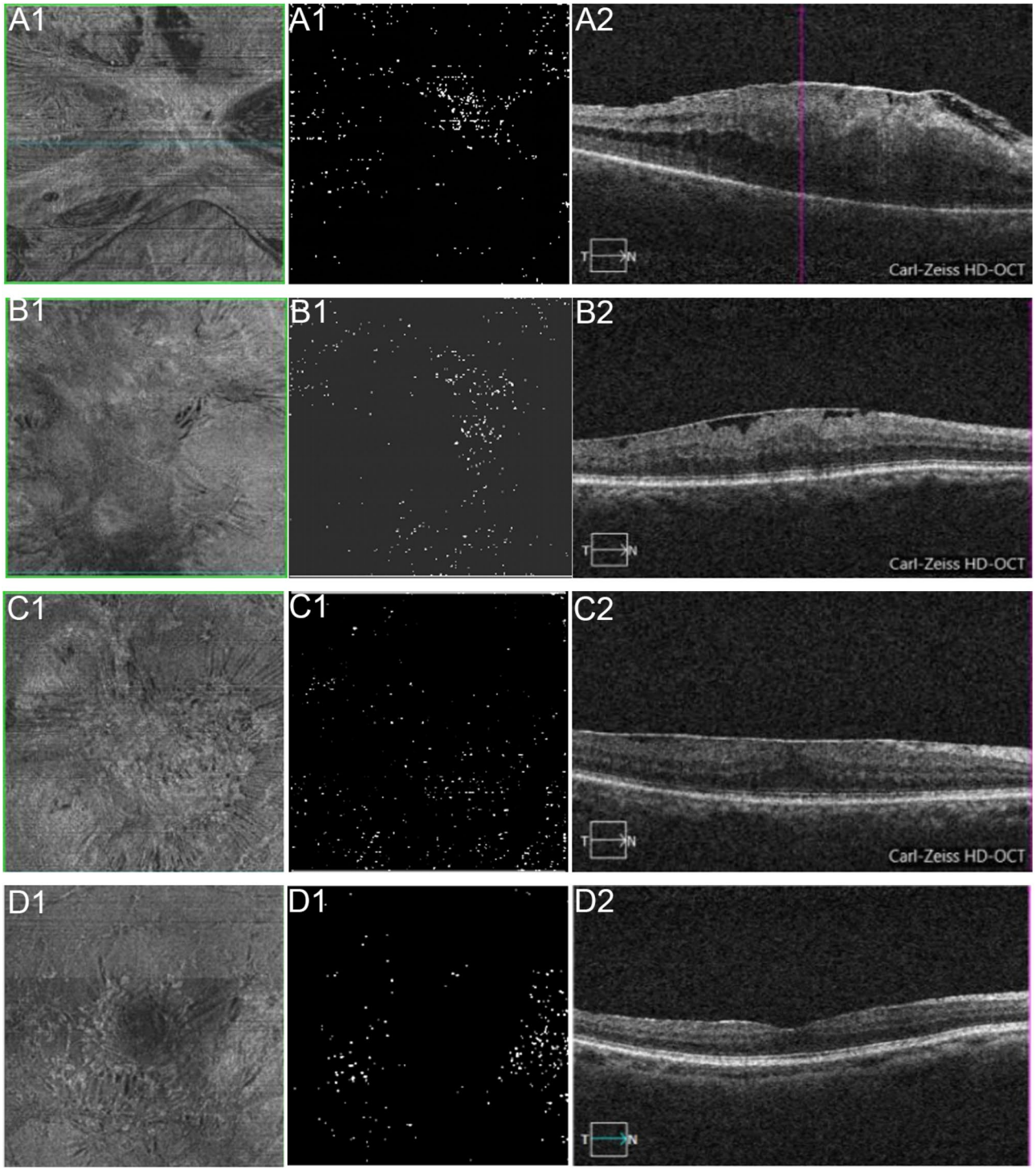

Fig. 2 Typical examples in stages. **A1**: Hyperreflective foci of the stage IV iERM after processing by ImageJ. **A2**: OCT image of the stage IV iERM. **B1**: Hyperreflective foci of the stage III iERM after processing by ImageJ. **B2**: OCT image of the stage III iERM. **C1**: Hyperreflective foci of the stage II iERM after processing by ImageJ. **C2**: OCT image of the stage II iERM. **D1**: Hyperreflective foci of the stage I iERM after processing by ImageJ. **D2**: OCT image of the stage I iERM

Nevertheless, the latter showed higher values than those between Stage I and Stage II. As the stage increased, the level of CMT also increased steadily, with significant differences observed among the four groups. The grading of the Stage exhibited a negative correlation with the FAZ indexes. The latter gradually declined with the increase of Stage level ($P<0.001$). Furthermore, SVD and SPD of different Stags displayed a significant correlation.

Specifically, Stage III and IV presented higher statistical significance compared to Stage I and stage II.

Correlation between hyperreflective foci and patient parameters

Hyperreflective foci counts and densities displayed significant individual variations. Univariate correlation analyses were conducted between hyperreflective foci parameters in all iERM patients and factors such as gender, age, OCTA, and OCT parameters. Hyperreflective foci area percentage and hyperreflective foci density exhibited no significant correlations with gender and age. However, hyperreflective foci area percentage and hyperreflective foci density showed significant correlations with CMT, FAZ area, and FAZ perimeter ($p < 0.005$). Specifically, CMT strongly positively correlated with hyperreflective foci density, hyperreflective foci count, and hyperreflective foci percentage, with r-values of 0.765,0.457,0.764, respectively. Although SVD showed only weak correlation with hyperreflective foci counts and hyperreflective foci density, FAZ area and FAZ perimeter demonstrated a significant negative correlation with hyperreflective foci counts, hyperreflective foci percentage, and hyperreflective foci density ($P < 0.001$). Additionally, the correlation between SVD and hyperreflective foci density was insignificant ($P > 0.05$). It is important to note that technical terms such as MLC and SVD are explained when first used to improve comprehensibility (Table 3)(Fig. 3).

Discussion

This study represents is a pioneering effort in utilizing en face OCTA images for investigating changes in hyperreflective foci at the retinal vitreous interface in eyes with idiopathic epiretinal membranes (iERM). In this study, we observed variations in the density and distribution of hyperreflective foci among patients afflicted with iERM at different stages.

A substantial body of evidence indicates that the inflammatory response plays a in the pathological process of iERM. According to Joshi et al. [10] and Zhao et al. [11], the primary cell types in iERM are hyalocytes and müller cells. Hyalocytes are classified as macrophages a kind of inflammation cells [12]. Glial cells in the iERM tissue express some trophic factor receptors and transcription factors, such as NF-kappaB, suggesting that glial cell signaling is involved in the development of the iERM, and whether there is a difference in the various stages of its development needs to be further investigated. Müller cells, microglia, and hyaloid cells are closely related to the development of iERM. It has been found that the internal limiting membrane tissue torn off during iMEM is predominantly glial and contains a variety of cells such as vitreous, retinal pigment epithelium (RPE) cells, macrophage-like cells, fibroblasts, and myofibroblasts, and often residual anterior membrane tissue. and myofibroblasts, among others, and often with remnants of adventitial tissue. Our results show that the increased count and altered distribution patterns of hyperreflective foci, as observed in OCT en face images, provide compelling evidence of their critical role in the pathophysiological progression of iERM. Remarkably, as the developmental stages of iERM unfold, we have observed corresponding changes in hyperreflective foci density and distribution, thereby underscoring an intimate association between hyperreflective foci activation and aggregation and the specific stage of iERM development. Despite significant variations in cell counts among individuals, it is noteworthy that cell numbers increase in conjunction with higher iERM grades.

Moreover, this study has successfully determined a positive correlation between posterior vitreous detachment (PVD) and the density of hyperreflective foci in iERM. PVD stands as the most critical factor in the pathogenesis of iERM, with a staggering 80–95% of iERM cases being intricately linked to PVD [12]. During the process of PVD formation, it has been observed that neuroglial acidic proteins and vitreous wafers exert specific influences on immature neuroglial cells, stellate glial cells, and mesenchymal cells. The residual vitreous cortex forms a

Table 3 Correlation between hyperreflective fociand patient parameters

Variables	hyperreflective foci density	hyperreflective foci count	hyperreflective foci percentage
gender	$r=0.132, p=0.256$	$r=0.239, p=0.118$	$r=-0.144, p=0.303$
age	$r=0.054, p=0.701$	$r=0.056, p=0.717$	$r=-0.088, p=0.568$
BCVA(LogMAR)	$r=0.117, p=0.368$	$r=0.821, p=0.000$	$r=0.534, p=0.003$
PVD	$r=0.302, P=0.043$	$r=0.311, p=0.037$	$r=0.262, P=0.082$
CMT	$r=0.765, p=0.000$	$r=0.457, p=0.00$	$r=0.764, p=0.000$
Faz area	$r=-0.559, p=0.001$	$r=-0.720, p=0.00$	$r=-0.599, p=0.003$
Faz perimeter	$r=-0.632, p=0.000$	$r=-0.686, p=0.00$	$r=-0.568, p=0.005$
SVD	$r=0.215, p=0.229$	$r=0.368, p=0.084$	$r=0.094, p=0.669$
SPD	$r=0.282, p=0.112$	$r=0.472, p=0.022$	$r=0.199, p=0.363$

BCVA: best-corrected visual acuity, PVD: posterior vitreous detachment, CMT: Central Macular Thickness, FAZ: foveal avascular zone, SVD: superficial vascular density, SPD: superficial perfusion density

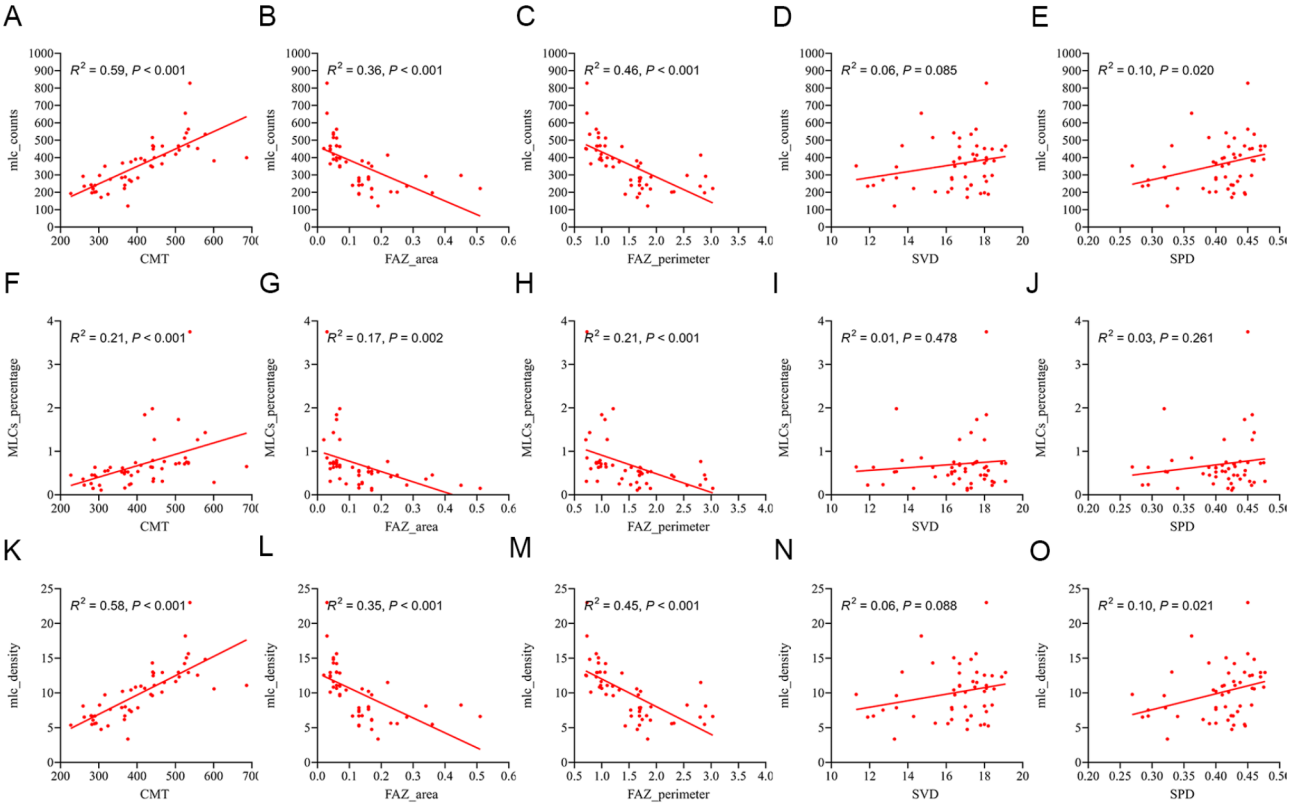

Fig. 3 Scatter plots illustrating the correlation between and patient parameters was assessed in this study. The association between CMT and hyperreflective foci counts(**A**), hyperreflective foci percentage(**F**), hyperreflective foci density (**k**) was found to be positive; **A** negative association was observed between the FAZ area and hyperreflective foci counts(**B**), hyperreflective foci percentage(**G**), hyperreflective foci density (**L**); The hyperreflective foci counts(**C**), hyperreflective foci percentage(**H**), hyperreflective foci density (**M**) exhibited **a** negative correlation with the FAZ perimeter. Notably, the SPD demonstrated a positive association with hyperreflective foci counts(**E**), hyperreflective foci percentage(**J**), hyperreflective foci density (**O**)

delicate layer on the macular surface and contains vitreous cells, including hyalocytes. It serves both as a structural component and a nurturing medium, activating tissue repair mechanisms [13]. Consequently, this results in the retention, migration, and proliferation of glial cells and hyalocytes on the macular surface. Hyalocytes stimulate Müller cells to migrate or proliferate, utimately leading to the formation of the complete internal limiting membrane (ILM) and the subsequent development of the epiretinal membrane [14]. Jacob et al. have detected the presence of macrophage-like cells on the retinal surface subsequent to PVD, thereby signifying the existence of neuroglial cells that either persist or migrate from the residual vitreous cortex on the retinal surface [15].

This study intriguing found a positive association between the density of hyperreflective foci and central macular thickness (CMT) of ERM. Prior studies have established the involvement of inflammatory responses in the pathological progression of iERM [16]. In addition, the growth of iERM is closely associated with the proliferation, migration, and phenotypic transformation of Müller cells [17]. It is postulated that the increasing density of hyperreflective foci, as indicated by the increasing EIFL grades, can be attributed to the persistent traction exerted by iERM, which causes centripetal mechanical displacement of the inner retinal layers. Concurrently, this traction exerts its influence on the normal Müller cells. Romano et al. Suggest that this effect triggers the migration and transformation of Müller cells, thereby activating them through the overexpression of glial fibrillary acidic protein (GFAP) [18]. Perturbations in nutrient availability and higher cytokine levels contribute to the development of ERM. Therefore, reactive proliferation of inner retinal glial cells ensues. The relationship between the proliferation of inner retinal glial cells and physical traction culminates in the formation of continuous ectopic inner foveal layers (CEIF), thereby giving rise to structural aberrations within the central fovea pertaining to the inner retinal layers [19]. Our data demonstrate that hyperreflective foci are correlated with CMT, but do not demonstrate causality.

Additionally, this study indicates a correlation between the increased count of hyperreflective foci and BCVA. Hyperreflective foci could also be microglia. Microglia, which are retinal macrophages, inhIbit both the inner and outer plexiform layers, and occasionally extend their

to the retinal nerve fiber layer [20, 21]. Therefore, this phenomenon results in fibrotic contraction and distortion of the customary tissue architecture, thereby inducing retinal thickening, disruption, and changes in the central foveal morphology, thus precipitating a decline in BCVA [22].

An association between metrics of hyperreflective foci and the superficial capillary plexus (SCP) in iERM was not identified in our study. This observation aligns with the findings of Zeng et al. [23], who also reported a lack of correlation between MLC density and SCP in patients with RVO. The retinal vascular plexus consists of the superficial SCP and the DCP, with the SCP situated in the ganglion cell layer and nerve fiber layer, while the DCP is located in the inner nuclear layer [24]. The mechanical traction exerted by iERM primarily affects the superficial retinal layers [22]. However, in terms of compromised blood flow, the DCP may be more susceptible to ischemic effects resulting from the increased presence of inflammatory cells due to iERM. Therefore, the impact of mechanical stress induced by iERM may have more profound consequences on the DCP than on the SCP [24, 25]. In addition, our observations indicate that hyperreflective foci in stage I and stage II iERM are predominantly situated at the periphery of the proliferative membrane. In contrast, in stage III and stage IV iERM, hyperreflective foci are not only found at the periphery but also concentrated in the central area of the proliferative membrane. This phenomenon can be attributed to the fact that stage I and stage II iERM do not disrupt the inner retinal structure. Conversely, in stage III and stage IV iERM, there is inner retinal ectopia at the central fovea, which adversely affects deep-layer blood flow, leading to hypoxia. This activation of retinal macrophages in the inner and outer plexiform layers may be the underlying cause [26]. Therefore, while no correlation was established between SCP and hyperreflective foci, further study is necessitated to determine whether a relationship exists with the DCP.

There are some limitations to our study. Firstly, a retrospective cross-sectional design was employed, resulting in inevitable biases in the obtained results. Secondly, the sample size was relatively small, and no subsequent statistical analysis was performed. The study was limited to analyzing the distribution and density of hyperreflective foci, without exploring their morphological aspects. Moreover, more precise techniques such as immunofluorescence staining or transmission electron microscopy (TEM) analysis were not utilized, and a comprehensive characterization of hyperreflective foci across different grades of iERM was not provided. Future research should seek to address these limitations by incorporating larger sample sizes and employing more comprehensive methodologies to further explain the histological characteristics of hyperreflective foci in iERM and speculate on the underlying pathogenesis. There is no indication of how HRF and iERM develop over time based on disease progression to assess causality. In addition, due to equipment constraints, this study did not assess the correlation between DCP and hyperreflective foci, which warrants exploration in future studies.

Conclusions

In summary, hyperreflective foci may be inflammatory cells. It has been determined that hyperreflective foci represent a simple and non-invasive method for assessing the severity of inflammatory reactions in all stages of iERM. Hyperreflective foci have been observed at all stages of iERM. In addition, this study has identified associations between hyperreflective foci and parameters such as PVD, CMT, FAZ area, and BCVA.

Acknowledgements
Not applicable.

Author contributions
JZ provided guidance and overall direction throughout the study design, paper writing and revision. SZ handled the literature review, data collection, data analysis and interpretation, and manuscript writing. YW provided expertise on data collection and review the manuscript. JH collected data and reviewed the manuscript. XL collected data and provided guidance on writing. All authors contributed to the article and approved the submitted version.

Funding
None.

Data availability
The raw data supporting the conclusions of this article can be provided upon reasonable request to authors.

Declarations

Ethics approval and consent to participate
This study was conducted in accordance with the guidelines of the Declaration of Helsinki. The studies involving human participants were reviewed and approved by Foshan Eyer Eye Ethics Committee (2023-IRB6).

Consent for publication
Not Applicable.

Competing interests
The authors declare no competing interests.

Received: 22 May 2024 / Accepted: 18 February 2025
Published online: 25 February 2025

References
1. Cho Kwan Hyuk, Woo Se Joon, Park Kyu Hyung. Correlation between inner-retinal changes and outer-retinal damage in patients with idiopathic epiretinal membrane. Retina. 2018;38(12):2327–35. https://doi.org/10.1097/IAE.0000000000001875
2. Xiaoyun XWC, Zhuoting Y et al. Prevalence and risk factors of epiretinal membranes: a systematic review and meta-analysis of population-based studies. BMJ Open. 2017;7(9):e014644. https://doi.org/10.1136/bmjopen-2016-014644

3. Sebag J. Anomalous posterior vitreous detachment: a unifying concept in vitreo-retinal disease. Graefes Arch Clin Exp Ophthalmol. 2014;242(8):690–8. https://doi.org/10.1007/s00417-004-0980-1
4. Castanos Maria V, Zhou Davis B, Linderman Rachel E, et al. Imaging of macrophage-like cells in living human retina using clinical OCT. Invest Ophthalmol Vis Sci. 2020;61(6):48. https://doi.org/10.1167/iovs.61.6.48
5. Wang Jacob M, Ong Janice X, Nesper Peter L, et al. Macrophage-like cells are still detectable on the retinal surface after posterior vitreous detachment. Sci Rep. 2022;12(1):12864. https://doi.org/10.1038/s41598-022-17229-5
6. Prinz Marco J, Steffen PJ. Microglia biology: one century of evolving concepts. Cell. 2019;179(2):292–311. https://doi.org/10.1016/j.cell.2019.08.053
7. Mafi M, Govetto A, Mahmoudinezhad G, et al. Pathogenesis of ectopic inner foveal layers (EIFL) and its impact on visual recovery after epiretinal membrane peeling. Retina-J Ret Vit Dis. 2025. https://doi.org/10.1097/IAE.0000000000004418
8. Santos AR, Ghate S, Lopes M, et al. ETDRS grading with CLARUS ultra-widefield images shows agreement with 7-fields colour fundus photography. BMC Ophthalmol. 2024;24(1):387. https://doi.org/10.1186/s12886-024-03537-z
9. Ong Janice X, Nesper Peter L, Fawzi Amani A, et al. Macrophage-like cell density is increased in proliferative diabetic retinopathy characterized by optical coherence tomography angiography. Invest Ophthalmol Vis Sci. 2021;62(10):2. https://doi.org/10.1167/iovs.62.10.2
10. Joshi M, Agrawal S, Christoforidis JB. Inflammatory mechanisms of idiopathic epiretinal membrane formation. Mediators Inflamm. 2013;2013:1–6. https://doi.org/10.1155/2013/192582
11. Zhao F, Gandorfer A, Haritoglou C, et al. Epiretinal cell proliferation in macular pucker and vitreomacular traction syndrome: analysis of flatmounted internal limiting membrane specimens. Retina. 2013;33:77–88. https://doi.org/10.1097/IAE.0b013e3182602087
12. Oscar MJVO-M, Rebecca Z, et al. Imaging of vitreous cortex hyalocyte dynamics using non-confocal quadrant-detection adaptive optics scanning light ophthalmoscopy in human subjects. Biomed Opt Express. 2022;13(3):1755–73. https://doi.org/10.1364/BOE.449417
13. Gandorfer A, Rohleder M, Kampik A. Epiretinal pathology of vitreomacular traction syndrome. Br J Ophthalmol. 2022;86(8):902–9. https://doi.org/10.1136/bjo.86.8.902
14. Gandorfer Arnd H, Christos S, Renate S, Ricarda Z, Fei K, Anselm. Residual cellular proliferation on the internal limiting membrane in macular pucker surgery. Retina. 2012;32(3):477–85. https://doi.org/10.1097/IAE.0b013e3182246e2a
15. Sun G, Xu A, Yang X, et al. Uncovering hidden patterns: macrophage-like cell distribution across different stages of posterior vitreous detachment. RETINA-J RET VIT DIS. 2024. https://doi.org/10.1097/IAE.0000000000004358
16. Dong Yoko K, Atsuhiro N, Kousuke, et al. Pathologic roles of receptor-associated prorenin system in idiopathic epiretinal membrane. Sci Rep. 2017;7(undefined):44266. https://doi.org/10.1038/srep44266
17. Romano Mario R, Ilardi Gennaro F, Mariantonia, et al. Intraretinal changes in idiopathic versus diabetic epiretinal membranes after macular peeling. PLoS ONE. 2018;13(5):e0197065. https://doi.org/10.1371/journal.pone.0197065
18. Doguizi Sibel SM, Ali O, Dilara, et al. Clinical significance of ectopic inner foveal layers in patients with idiopathic epiretinal membranes. Eye (Lond). 2018;32:1652–60. https://doi.org/10.1038/s41433-018-0153-9
19. O'Koren EG, Mathew R, Saban DR. Fate mapping reveals that microglia and recruited monocyte-derived macrophages are definitively distinguishable by phenotype in the retina. Sci Rep. 2016;6(undefined):20636. https://doi.org/10.1038/srep20636
20. O'Koren Emily G, Chen Y, Mikael K, et al. Microglial function is distinct in different anatomical locations during retinal homeostasis and degeneration. Immunity. 2019;50(3):723–e7377. https://doi.org/10.1016/j.immuni.2019.02.007
21. Schuster Ronen Y, Fereshteh E, Maya, et al. The role of myofibroblasts in physiological and pathological tissue repair. Cold Spring Harb Perspect Biol. 2023;15(1):undefined. https://doi.org/10.1101/cshperspect.a041231
22. Zeng Y, Zhang X, Mi L, Ji Y, Zhuang X, He G, et al. Macrophage-like cells characterized by En face optical coherence tomography was associated with fluorescein vascular leakage in Behç Et's uveitis. Ocular Immunol Inflamm. 2022:1–7. https://doi.org/10.1080/09273948.2022.2080719
23. Spaide RF, Klancnik JM Jr, Cooney MJ. Retinal vascular layers imaged by fluoresce in angiography and optical coherence tomography angiography. JAMA Ophthalmol. 2015;133(1):45–50. https://doi.org/10.1001/jamaophthalmol.2014.3616
24. Werner Jens U, Dreyhaupt, Jens, Enders Christian. Evaluation of automated measurement of macular ischemic changes in retinal vein occlusion with optical coherence tomography angiography. Ophthalmic Surg Lasers Imaging Retina. 2023;54(8):462–9. https://doi.org/10.3928/23258160-20230707-01
25. Feng Jingyang Y, Xiaotong X, Mengqiao, et al. Association of microvasculature and macular sensitivity in idiopathic macular epiretinal membrane: using OCT angiography and microperimetry. Front Med (Lausanne). 2021;8(undefined):655013. https://doi.org/10.3389/fmed.2021.655013
26. Fragiotta S, Abdolrahimzadeh S, Dolz-Marco R, Sakurada Y, Orly Gal-Or, Gianluca Scuderi. Significance of hyperreflective foci as an optical coherence tomography biomarker in retinal diseases: characterization and clinical implications. J Ophthalmol. 2021;10. https://doi.org/10.1155/2021/6096017

Publisher's note